Uncertainty Analysis of NIST's 20 Liter Hydrocarbon Liquid Flow Standard

Aaron N. Johnson
NIST Fluid Metrology Group
100 Bureau Drive
Gaithersburg, MD 20899
301-975-5954
Aaron.Johnson@nist.gov

Chris J. Crowley
NIST Fluid Metrology Group
100 Bureau Drive
Gaithersburg, MD 20899
301-975-4648
Chris.Crowley@nist.gov

TT Yeh
NIST Fluid Metrology Group
100 Bureau Drive
Gaithersburg, MD 20899
301-975-5953
TTYeh@nist.gov

Abstract: The National Institute of Standards and Technology (NIST) uses a bi-directional 20 L-displacement piston prover as its primary standard for measuring hydrocarbon liquid flows ranging from 1.86×10^{-5} m^3/s (0.3 gpm) to 2.6×10^{-3} m^3/s (40 gpm). Our analysis that shows that the prover's uncertainty over this flow range is 0.074 % (k = 2, corresponding to a 95 % confidence interval). Using a dual rotor turbine meter as the transfer standard, we compare the new 20 L piston prover standard with NIST's other hydrocarbon liquid standards and NIST's water flow standard. The results are consistent with the presented uncertainty analysis.

Keyword: NIST liquid hydrocarbon flow standard, piston prover, water draw procedure, liquid flow calibration, uncertainty analysis

1. Introduction

NIST measures liquid hydrocarbon flows using the four primary standards listed in Table 1. NIST's customers establish traceability to the SI unit of flow by calibrating their meter against these U.S. national standards. These standards accommodate all types of pulse producing flowmeters, although turbine meters are the most frequently calibrated at NIST. The first two standards listed in Table 1 (*i.e.*, the Small and Large Cox Bench) work on a gravimetric principle whereby the flow is determined by weighing the mass of liquid collected in a tank during a measured time interval. The latter two primary standards are the 2 L Hydrocarbon Liquid Flow Standard (2 L HLFS) and the newly developed 20 L Hydrocarbon Liquid Flow Standard (20 L HLFS). These piston prover standards work on a volumetric principle whereby the piston displaces a known volume of fluid during a measured time interval. The first three standards in Table 1 have been in use for several years and their operation and uncertainty analyses are documented in NIST internal records and in previous publications [1, 2]. In this manuscript, we document the operating principle for the 20 L HLFS, its governing flow equations, calibration procedure, uncertainty analysis, and the results of comparisons with the three older NIST liquid hydrocarbon flow standards and also with NIST's Water Flow Calibration Facility [3].

Table 1. *Capabilities of NIST's four Hydrocarbon Liquid Flow Standards. Flow standards are used with Stoddard solvent (i.e., MIL-C-7024 B Type II) or fluids with similar kinematic viscosities.*[i, ii]

NIST Primary Flow Standard	Flow Range	Expanded Uncertainty		Absolute Pressure Range	Temperature Range
		Volumetric Flow	Mass Flow		
Small Cox Bench	0.05 to 8 lpm (0.014 to 2.1 gpm)	0.12 %	0.12 %	150 kPa to 250 kPa	14ºC to 30ºC
Large Cox Bench	5.3 to 918 lpm (1.4 to 242 gpm)	0.12 %	0.12 %	150 kPa to 250 kPa	14ºC to 30ºC
2 L HLFS (small piston prover)	0.19 to 5.7 lpm (0.05 to 1.5 gpm)	0.04 %	0.05 %	150 kPa to 380 kPa	21ºC to 23ºC
20 L HLFS (medium piston prover)	1.1 to 151 lpm (0.3 to 40 gpm)	0.074 %	0.08 %	150 kPa to 380 kPa	21ºC to 23ºC

2. NIST's 20 L HLFS

2.1. Description of the 20 L HLFS

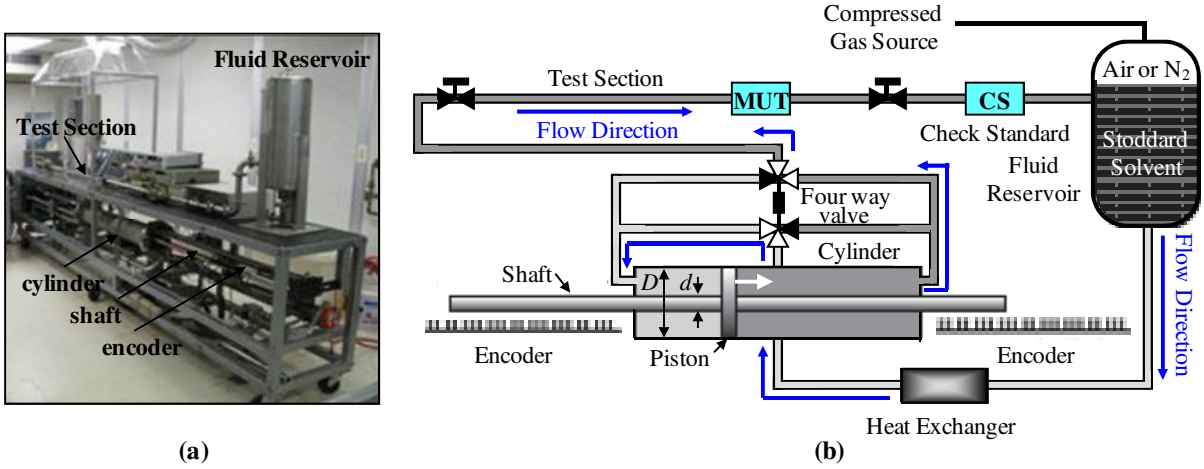

Figure 1. *Photograph and drawing of the essential components of the 20 L HLFS*

The photograph in Fig. 1a shows the major components of the 20 L HLFS and the diagram in Fig. 1b shows the flow path of the calibration fluid throughout the prover assembly when the piston is stroking to the right. As the piston strokes rightward the flow exits the cylinder on the right side and moves through the upper section of the four-way valve into the test section. The meter under test (MUT) is calibrated using the known flow delivered from piston-cylinder assembly as the reference.

---

[i] Throughout this document the units lpm are actual liters per minute. Divide lpm by 60000 to convert to m^3/s and divide lpm by 3.785412 to convert to gallons per minute which is abbreviated gpm herein.

[ii] Uncertainty values at approximately the 95 % confidence interval having a coverage factor of two ($k = 2$). These uncertainties do not include repeatability, reproducibility, and hysteresis of the flowmeter being calibrated. These additional uncertainty components are assessed during a flowmeter calibration and are documented in a report of calibration.

The data collected during a flowmeter calibration is verified against a turbine meter check standard installed downstream of the MUT. Fluid leaving the test section enters into a fluid reservoir where a compressed gas source applies pressure to the fluid. The applied pressure helps prevent cavitation on the turbine meter blades of NIST's check standard as well customer turbine meters. As the flow exits the reservoir it is directed through a heat exchanger and then around the piston-cylinder assembly to the lower section of the four-way valve. The flow loop is completed when the fluid reenters the left side of the cylinder. Flow continues to accumulate in the left side of the cylinder until the piston reaches the end of the rightward stroke, at which time the four-way valve is actuated and the piston strokes leftward. As illustrated in the Fig. 2, the four-way valve maintains unidirectional flow in the test section regardless of the direction of the piston stroke.

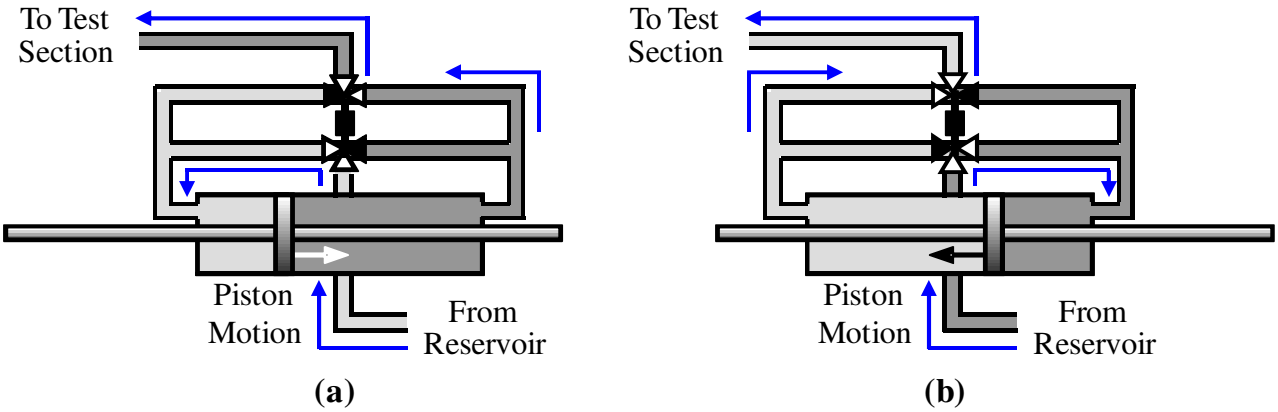

Figure 2. *Sketch showing the four-way valve positions and the corresponding flow directions for the piston stroking rightward (a) and leftward (b)*

The piston is driven using a servomotor and drive gear system that is coupled to the piston shaft. During each stroke, a feedback circuit controls the servomotor output so that the piston velocity quickly reaches a constant value equal to the desired flow set point divided by the cross sectional area. Data is collected only while the velocity is constant. A timing circuit measures the duration of the piston stroke (Δt) while the distance is measured by two redundant, linear encoders, each having a nominal encoder constant of $\Delta L_e' = 20$ µm/pulse (or 50 pulses/mm). The length of the piston stroke is the encoder constant multiplied by the average number of encoder pulses (N_e) from the two encoders. Each encoder gives two pulse counts (corresponding to the leading and trailing edge of a pulse) so that N_e is the average of four different encoder counts. During a typical NIST calibration, the piston stroke for each calibration point uses 85 % of the total cylinder length (corresponding to 85 % of the total cylinder volume) for flows ranging from 151 lpm down to 5.7 lpm. As shown in Table 2, the length of the piston stroke is reduced at lower flows so that the duration of the stroke is $\Delta t_{max} = 120$ s. The shafts on either side of the piston have nominal diameters of $d = 2.54$ cm, while the nominal cylinder diameter is $D = 15.24$ cm. The shaft and cylinder diameters are ground and polished so that the variation of the cross sectional area, $A_{cs} = \pi (D^2 - d^2)/4$, (along the cylinder length) is negligible compared with other uncertainties of the 20 L HLFS.

***Table 2**. Nominal characteristics of NIST's 20 L HLFS during a flow measurement*

Volumetric Flow [lpm]	Volumetric Flow [gpm]	Piston Velocity [cm/s]	Duration of Piston Stroke (Δt) [s]	Length of Piston Stroke [cm]	Encoder Pulses (N_e) [pulse]	Percent of Cylinder Volume Swept [%]
151.4	40	14.2	4.6	64.8	32410	85
113.6	30	10.7	6.1	64.8	32410	85
75.7	20	7.1	9.1	64.8	32410	85
37.9	10	3.5	18.2	64.8	32410	85
18.9	5	1.8	36.4	64.8	32410	85
9.46	2.5	0.9	72.8	64.8	32410	85
3.78	1	0.36	120.0	42.7	21361	56
1.1	0.3	0.11	120.0	12.8	6408	17

2.2. Flow Measurement Principle

Flow determinations are based on the piston displacing a known volume of fluid during a measured time interval. The volumetric flow exiting the cylinder is

$$Q_{\mathrm{cyl}} = \frac{K_{\mathrm{V}} N_{\mathrm{e}}}{\Delta t} \tag{1}$$

where K_{V} is the calibrator constant or herein called the *volumetric prover K-factor* with units of volume per encoder pulse. The *volumetric prover K-factor* equals[iii]

$$K_{\mathrm{V}} = A_{\mathrm{cs}} \Delta L'_{\mathrm{e}} \tag{2}$$

the cross sectional area multiplied by the encoder constant. This *K*-factor has a slight dependence on the fluid's operating temperature and pressure and on the room temperature. At different operating conditions, thermal expansion and forces related to pressure change the cylinder and shaft diameters, and consequently A_{cs}. Similarly, thermal expansion causes $\Delta L'_{\mathrm{e}}$ to change with the room temperature. Instead of characterizing K_{V} over the range of prover operating conditions, standard practice is to determine its value at a single reference temperature (T_{ref}) and pressure (P_{ref}), and correct volumetric flow calculations for *reference condition effects* using

$$D = D_{\mathrm{ref}} \left[1 + \alpha_{\mathrm{st}} \left(T - T_{\mathrm{ref}}\right)\right], \tag{3a}$$

$$d = d_{\mathrm{ref}} \left[1 + \alpha_{\mathrm{st}} \left(T - T_{\mathrm{ref}}\right)\right], \tag{3b}$$

$$\Delta L'_{\mathrm{e}} = \Delta L'_{\mathrm{e,ref}} \left[1 + \alpha_{\mathrm{en}} \left(T_{\mathrm{en}} - T_{\mathrm{ref}}\right)\right] \tag{3c}$$

[iii] The diameters of the shafts on either side of the piston are slightly different so that the cross sectional area differs when the piston sweeps to the left versus to the right. To accommodate this difference it is common practice to distinguish between the volumetric prover *K*-factor when the piston sweeps left ($K_{\mathrm{V,left}}$) versus when the piston sweeps right ($K_{\mathrm{V,right}}$).

where $\alpha_{st} = 1.7 \times 10^{-5}$ K^{-1} [4,5] is the linear expansion coefficient for the stainless steel cylinder and shafts, $\alpha_{en} = 8 \times 10^{-6}$ K^{-1} [5] is the linear expansion coefficient for the glass encoder scale, and T_{en} and T are the temperatures of the encoder and the fluid.[iv] Elastic deformation caused by pressure stresses can be neglected because the cylinder's cross sectional area changes by less 0.003 % at the maximum operating pressure. To minimize the uncertainties introduced by the linear temperature approximation used in Eqs. (3a), (3b) and (3c), the prover's operating conditions should be maintained close to T_{ref} and P_{ref}. In this way, the theoretically corrected reference condition effects are small relative to the measured K_v^{ref} values.

The three commonly used methods to determine the reference volumetric prover *K*-factor (K_v^{ref}) are 1) a water draw procedure [6], 2) dimensional measurements of the cylinder diameter (D_{ref}), the shaft diameters on either side of the piston (d_{ref}), and the encoder constant ($\Delta L'_{e,ref}$) [1], and 3) use of a transfer standard flowmeter [6]. In this work K_v^{ref} is determined using the water draw method at a reference condition of T_{ref} = 21 ℃ and P_{ref} = 101.325 kPa as explained in section 4.1.

2.3. Flow at the MUT under Ideal Conditions

When the prover is operated at the reference conditions the volumetric flow exiting the cylinder is $Q_{cyl}^{ref} = K_v^{ref} N_e / \Delta t$, and the mass flow is $\dot{m}_{cyl}^{ref} = \rho_{ref} K_v^{ref} N_e / \Delta t$ where ρ_{ref} is the fluid density evaluated at P_{ref} and T_{ref}. The objective of a piston prover standard is to determine the flow at the MUT using the known reference flows. However, the volumetric and mass flow at the MUT only equal the respective reference flows (*i.e.*, $Q_{MUT}^{ideal} = Q_{cyl}^{ref}$ and $\dot{m}_{MUT}^{ideal} = \dot{m}_{cyl}^{ref}$) under the following idealized conditions:

1) steady flow,
2) room temperature equal to T_{ref},
3) fluid temperature equal to T_{ref} throughout the cylinder and test section,
4) fluid pressure equals P_{ref} throughout the cylinder and test section, and
5) no leaks into or out of the volume starting at the piston and extending to the MUT.

NIST operates its 20 L HLFS as close as possible to these idealized conditions. Steady flow conditions are obtained by stroking the piston at a nearly constant velocity during data collection. The fluid temperature is controlled to T_{ref} using the heat exchanger shown in Fig. 1. Temperature uniformity of the fluid in the prover assembly is established by cycling the piston back and forth until the 5 temperature sensors distributed throughout the test section and the 2 temperature sensors located at the left and right exits of the piston-cylinder assembly agree to within 0.5 C or better. The room housing the 20 L HLFS is maintained to within ± 3 ℃ of the reference temperature to minimize heat transfer effects. The pressure is maintained only slightly above P_{ref} (*i.e.*, between 150 kPa and 380 kPa) to prevent measurement errors and possible damage caused by cavitation to customer turbine meters.

[iv] The fluid temperature is assumed to be in thermal equilibrium with the cylinder and shaft, and the encoder temperature is assumed equal to the room temperature.

Leaks only affect flow measurements when they are located between the piston and the MUT. Leaks in this region can be either external (*i.e.*, leakage from the prover to the room) or internal (*i.e.*, leakage past the four-way valve or past the piston). External leaks are visible and easily fixed. Internal leaks past the piston are prevented using two hydraulic wiper seals, one on either side of the piston. If either seal fails, apertures inside the piston drain the leak into the hollow piston shaft until the leak becomes visible when it drips onto the floor at the opposite end of the shaft. Leakage past the four-way valve is detected indirectly by monitoring the consistency of the check standard that is permanently installed in the test section. Because leaks are detected and repaired, errors resulting from undetected leaks are small enough to be neglected.

2.4. Corrections for Non-Ideal Operating Conditions

The ideal flow conditions listed in section 2.3 are never perfectly realized in practice. To improve flow measurement accuracy corrections are made to $Q_{\mathrm{MUT}}^{\mathrm{ideal}}$ and $\dot{m}_{\mathrm{MUT}}^{\mathrm{ideal}}$ to account for small deviations from the ideal conditions. In particular, corrections are made to account for non-idealities caused 1) by *reference condition effects* and 2) by *gradient effects* (*i.e.*, spatial non-uniformities in the temperature and/or pressure). Corrections for reference condition effects are made when the operating conditions (*i.e.*, fluid temperature, fluid pressure, and room temperature differ from T_{ref} and P_{ref}). These corrections account either for changes in the cylinder volume (as already discussed in section 2.2) or for changes in the fluid density. Density related corrections are made using a linear function of temperature and pressure

$$\rho = \rho_{\mathrm{ref}}\left[1-\beta\left(T-T_{\mathrm{ref}}\right)+\kappa\left(P-P_{\mathrm{ref}}\right)\right] \tag{4}$$

where β is the thermal expansion coefficient and κ is the isothermal compressibility factor (or the inverse of the isothermal bulk modulus). For Stoddard solvent the density is measured at ambient pressure over the operating temperature range of the piston prover with a vibrating tube densimeter. The parameters ρ_{ref} and β are fit coefficients of the measured data. Pressure corrections are made by calculating κ using the API standards.[7]

Pressure and temperature differences between the fluid exiting the cylinder and the fluid at the MUT cause the volumetric flow at these two locations to differ. These *gradient effects* are caused by pressure loss mechanisms such as wall friction, elbows, fittings, etc., as well as by heat transfer caused by temperature differences between the fluid and the room. Gradient effects are corrected by measuring the average temperature and pressure at the cylinder exit and at the MUT. [v] The measured temperatures and pressures can be used in Eq. (4) to calculate the density at the cylinder exit (ρ_{cyl}) and at the MUT (ρ_{MUT}). The volumetric flow at the MUT (for steady flow conditions) equals the measured density ratio ($\rho_{\mathrm{cyl}}/\rho_{\mathrm{MUT}}$) multiplied by the volumetric flow exiting the piston-cylinder.

A third type of non-ideality results when the flow is unsteady. In this case the mass flow exiting the cylinder is not equal to the mass flow at the MUT. The difference in mass flow is attributed to

[v] Currently NIST measures the pressure at the MUT, but not at the piston-cylinder exit. Consequently, the pressure correction factor G_2 shown in Table 3 (see Section 3.1) is not used to correct the volumetric flow, but is estimated and included in the uncertainty budget.

accumulation of mass in the unswept region of the cylinder and in the volume of piping connecting the cylinder exit and the MUT. That is, the mass in these volumes at the start of the piston stroke is not equal to mass at the end of the piston stroke. Although NIST does not currently correct for *mass storage effects*, we estimate the magnitude of these effects for each calibration and include them in the uncertainty budget.

In next section the mass conservation principle is used to derive expressions for the three types of corrections considered in this manuscript (*i.e.*, reference condition corrections, gradient corrections, and storage effect corrections).

3. Formulation of the Governing Flow Equations

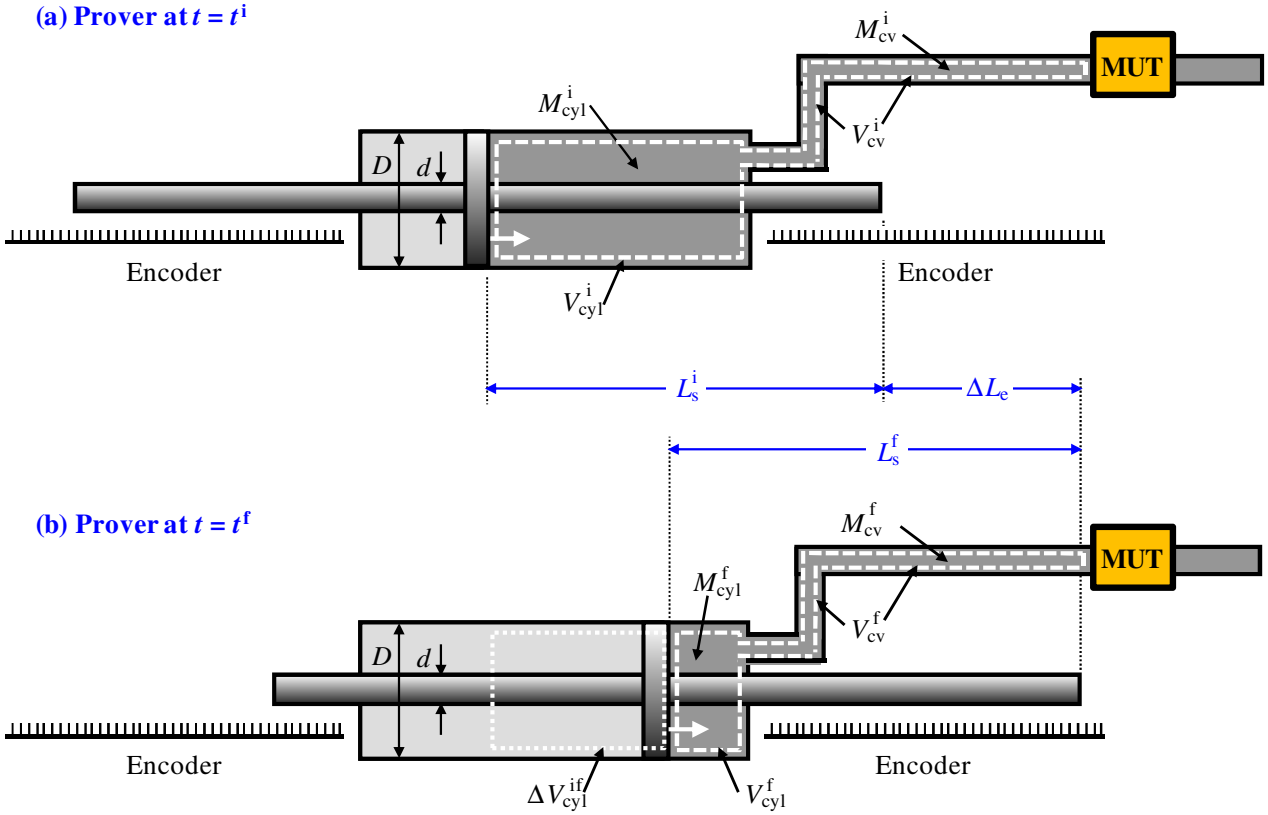

Figure 3. *Sketch showing the orientation of the piston before and after the piston stroke.*

Figures 3a and 3b show the location of the piston at the start of the measured time interval (t_i) and at the end of the measured time interval (t_f). The white dashed lines constitute the *control volume* where mass conservation is applied. The control volume includes the volume of fluid to the right of the piston inside the cylinder (V_{cyl}), and the fluid in the connecting volume between the exit of the cylinder and the MUT (V_{cv}). As the piston strokes rightward the size of the control volume decreases such that the time-averaged mass flow through the MUT is

$$\tilde{\dot{m}}_{MUT} = \frac{\Delta M_{cyl}^{if}}{\Delta t} + \frac{\Delta M_{cv}^{if}}{\Delta t} - \tilde{\dot{m}}_{leak} \tag{5}$$

where $\Delta M_{\mathrm{cyl}}^{\mathrm{if}} = M_{\mathrm{cyl}}^{\mathrm{i}} - M_{\mathrm{cyl}}^{\mathrm{f}}$ is the difference between the initial and final mass in the cylinder, $\Delta M_{\mathrm{cv}}^{\mathrm{if}} = M_{\mathrm{cv}}^{\mathrm{i}} - M_{\mathrm{cv}}^{\mathrm{f}}$ is difference between the initial and final mass in the connecting volume, $\Delta t = t^{\mathrm{f}} - t^{\mathrm{i}}$ is the measured time interval, and $\tilde{\dot{m}}_{\mathrm{leak}}$ is net time-averaged mass flow leaking out of the control volume. The mass terms in Eq. (5) can be replaced by the product of the spatially averaged density multiplied by volume (*e.g.*, $M_{\mathrm{cyl}}^{\mathrm{i}} = \hat{\rho}_{\mathrm{cyl}}^{\mathrm{i}} V_{\mathrm{cyl}}^{\mathrm{i}}$, $M_{\mathrm{cv}}^{\mathrm{i}} = \hat{\rho}_{\mathrm{cv}}^{\mathrm{i}} V_{\mathrm{cv}}^{\mathrm{i}}$) where for example $\hat{\rho}_{\mathrm{cyl}}^{\mathrm{i}}$ is the initial average density in the cylinder volume ($V_{\mathrm{cyl}}^{\mathrm{i}}$), and $\hat{\rho}_{\mathrm{cyl}}^{\mathrm{f}}$ is the final average density in the control volume ($V_{\mathrm{cyl}}^{\mathrm{f}}$). After this substitution time-averaged mass flow at the MUT is

$$\tilde{\dot{m}}_{\mathrm{MUT}} = \frac{\hat{\rho}_{\mathrm{cyl}}^{\mathrm{i}} V_{\mathrm{cyl}}^{\mathrm{i}} - \hat{\rho}_{\mathrm{cyl}}^{\mathrm{f}} V_{\mathrm{cyl}}^{\mathrm{f}}}{\Delta t} + \frac{\hat{\rho}_{\mathrm{cv}}^{\mathrm{i}} V_{\mathrm{cv}}^{\mathrm{i}} - \hat{\rho}_{\mathrm{cv}}^{\mathrm{f}} V_{\mathrm{cv}}^{\mathrm{f}}}{\Delta t} - \tilde{\dot{m}}_{\mathrm{leak}}$$

or

$$\tilde{\dot{m}}_{\mathrm{MUT}} = \left[\frac{\hat{\rho}^{\mathrm{i}} V^{\mathrm{i}} - \hat{\rho}^{\mathrm{f}} V^{\mathrm{f}}}{\Delta t}\right]_{\mathrm{cyl}} + \left[\frac{\hat{\rho}^{\mathrm{i}} V^{\mathrm{i}} - \hat{\rho}^{\mathrm{f}} V^{\mathrm{f}}}{\Delta t}\right]_{\mathrm{cv}} - \tilde{\dot{m}}_{\mathrm{leak}}\,. \tag{6}$$

By adding and subtracting the terms $\hat{\rho}_{\mathrm{cyl}}^{\mathrm{i}} V_{\mathrm{cyl}}^{\mathrm{f}}$ and $\hat{\rho}_{\mathrm{cv}}^{\mathrm{i}} V_{\mathrm{cv}}^{\mathrm{f}}$ to the right side of Eq. (6) the time-averaged mass flow (with no leaks) is

$$\begin{aligned}
\tilde{\dot{m}}_{\mathrm{MUT}} &= \left[\frac{\hat{\rho}^{\mathrm{i}} V^{\mathrm{i}} - \hat{\rho}^{\mathrm{f}} V^{\mathrm{f}} + \left(\hat{\rho}^{\mathrm{i}} V^{\mathrm{f}} - \hat{\rho}^{\mathrm{i}} V^{\mathrm{f}}\right)}{\Delta t}\right]_{\mathrm{cyl}} + \left[\frac{\hat{\rho}^{\mathrm{i}} V^{\mathrm{i}} - \hat{\rho}^{\mathrm{f}} V^{\mathrm{f}} + \left(\hat{\rho}^{\mathrm{i}} V^{\mathrm{f}} - \hat{\rho}^{\mathrm{i}} V^{\mathrm{f}}\right)}{\Delta t}\right]_{\mathrm{cv}} \\
&= \left[\frac{\left(\hat{\rho}^{\mathrm{i}} V^{\mathrm{i}} - \hat{\rho}^{\mathrm{i}} V^{\mathrm{f}}\right) + \left(\hat{\rho}^{\mathrm{i}} V^{\mathrm{f}} - \hat{\rho}^{\mathrm{f}} V^{\mathrm{f}}\right)}{\Delta t}\right]_{\mathrm{cyl}} + \left[\frac{\left(\hat{\rho}^{\mathrm{i}} V^{\mathrm{i}} - \hat{\rho}^{\mathrm{i}} V^{\mathrm{f}}\right) + \left(\hat{\rho}^{\mathrm{i}} V^{\mathrm{f}} - \hat{\rho}^{\mathrm{f}} V^{\mathrm{f}}\right)}{\Delta t}\right]_{\mathrm{cv}} \\
&= \left[\frac{\hat{\rho}^{\mathrm{i}} \Delta V^{\mathrm{if}} + \Delta\hat{\rho}^{\mathrm{if}} V^{\mathrm{f}}}{\Delta t}\right]_{\mathrm{cyl}} + \left[\frac{\hat{\rho}^{\mathrm{i}} \Delta V^{\mathrm{if}} + \Delta\hat{\rho}^{\mathrm{if}} V^{\mathrm{f}}}{\Delta t}\right]_{\mathrm{cv}} \\
&= \frac{\hat{\rho}_{\mathrm{cyl}}^{\mathrm{i}} \Delta V_{\mathrm{cyl}}^{\mathrm{if}}}{\Delta t} + \frac{V_{\mathrm{cyl}}^{\mathrm{f}} \Delta\hat{\rho}_{\mathrm{cyl}}^{\mathrm{if}}}{\Delta t} + \frac{\hat{\rho}_{\mathrm{cv}}^{\mathrm{i}} \Delta V_{\mathrm{cv}}^{\mathrm{if}}}{\Delta t} + \frac{V_{\mathrm{cv}}^{\mathrm{f}} \Delta\hat{\rho}_{\mathrm{cv}}^{\mathrm{if}}}{\Delta t}
\end{aligned}$$

$$\tilde{\dot{m}}_{\mathrm{MUT}} = \left(\frac{\hat{\rho}_{\mathrm{cyl}}^{\mathrm{i}} \Delta V_{\mathrm{cyl}}^{\mathrm{if}}}{\Delta t}\right)\left[1 + \frac{V_{\mathrm{cyl}}^{\mathrm{f}}}{\Delta V_{\mathrm{cyl}}^{\mathrm{if}}}\frac{\Delta\hat{\rho}_{\mathrm{cyl}}^{\mathrm{if}}}{\hat{\rho}_{\mathrm{cyl}}^{\mathrm{i}}} + \frac{V_{\mathrm{cv}}^{\mathrm{f}}}{\Delta V_{\mathrm{cyl}}^{\mathrm{if}}}\frac{\Delta\hat{\rho}_{\mathrm{cv}}^{\mathrm{if}}}{\hat{\rho}_{\mathrm{cyl}}^{\mathrm{i}}} + \frac{\hat{\rho}_{\mathrm{cv}}^{\mathrm{i}}}{\hat{\rho}_{\mathrm{cyl}}^{\mathrm{i}}}\frac{\Delta V_{\mathrm{cv}}^{\mathrm{if}}}{\Delta V_{\mathrm{cyl}}^{\mathrm{if}}}\right] \tag{7}$$

where $\Delta V_{\mathrm{cyl}}^{\mathrm{if}} = V_{\mathrm{cyl}}^{\mathrm{i}} - V_{\mathrm{cyl}}^{\mathrm{f}}$ is the volume swept by the piston during the measurement interval indicated by the dotted lines in Fig. 3b. The terms in the square brackets account for mass storage effects in the portion of the cylinder volume not swept by the piston ($V_{\mathrm{cyl}}^{\mathrm{f}}$) shown in Fig. 3b, and in the connecting volume (V_{cv}). Here, $\Delta\hat{\rho}_{\mathrm{cyl}}^{\mathrm{if}} = \hat{\rho}_{\mathrm{cyl}}^{\mathrm{i}} - \hat{\rho}_{\mathrm{cyl}}^{\mathrm{f}}$ and $\Delta\hat{\rho}_{\mathrm{cv}}^{\mathrm{if}} = \hat{\rho}_{\mathrm{cv}}^{\mathrm{i}} - \hat{\rho}_{\mathrm{cv}}^{\mathrm{f}}$ are the change in density in the cylinder volume and in the connecting volume between the start (t^{i}) and stop (t^{f}) of

the timing interval. These density changes correspond to changes in the average temperature and/or pressure in these volumes between the start and stop of the timing interval (*i.e.*, $\hat{T}^{\mathrm{i}}_{\mathrm{cyl}} \neq \hat{T}^{\mathrm{f}}_{\mathrm{cyl}}$, $\hat{T}^{\mathrm{i}}_{\mathrm{cv}} \neq \hat{T}^{\mathrm{f}}_{\mathrm{cv}}$, $\hat{P}^{\mathrm{i}}_{\mathrm{cyl}} \neq \hat{P}^{\mathrm{f}}_{\mathrm{cyl}}$, and $\hat{P}^{\mathrm{i}}_{\mathrm{cv}} \neq \hat{P}^{\mathrm{f}}_{\mathrm{cv}}$). Temporal changes in the average temperature and pressure in the connecting volume can also alter the connecting volume size ($V^{\mathrm{i}}_{\mathrm{cv}} \neq V^{\mathrm{f}}_{\mathrm{cv}}$) via thermal expansion and elastic deformation caused by pressure forces. However, changes in the connecting volume ($\Delta V^{\mathrm{if}}_{\mathrm{cv}} = V^{\mathrm{i}}_{\mathrm{cv}} - V^{\mathrm{f}}_{\mathrm{cv}}$) are generally negligible relative to density related changes.

The time-averaged volumetric flow at the MUT is determined by dividing Eq. (7) by the density at the MUT

$$\tilde{Q}_{\mathrm{MUT}} = \left(\frac{\Delta V^{\mathrm{if}}_{\mathrm{cyl}}}{\Delta t}\right)\left[\frac{\hat{\rho}^{\mathrm{i}}_{\mathrm{cyl}}}{\tilde{\rho}_{\mathrm{MUT}}} + \frac{V^{\mathrm{f}}_{\mathrm{cyl}}}{\Delta V^{\mathrm{if}}_{\mathrm{cyl}}}\frac{\Delta\hat{\rho}^{\mathrm{if}}_{\mathrm{cyl}}}{\tilde{\rho}_{\mathrm{MUT}}} + \frac{V^{\mathrm{f}}_{\mathrm{cv}}}{\Delta V^{\mathrm{if}}_{\mathrm{cyl}}}\frac{\Delta\hat{\rho}^{\mathrm{if}}_{\mathrm{cv}}}{\tilde{\rho}_{\mathrm{MUT}}} + \frac{\hat{\rho}^{\mathrm{i}}_{\mathrm{cv}}}{\tilde{\rho}_{\mathrm{MUT}}}\frac{\Delta V^{\mathrm{if}}_{\mathrm{cv}}}{\Delta V^{\mathrm{if}}_{\mathrm{cyl}}}\right]. \tag{8}$$

As expected, the mass flow in Eq. (7) and the volumetric flow in Eq. (8) simplify to $\dot{m}^{\mathrm{ideal}}_{\mathrm{MUT}} = \dot{m}^{\mathrm{ref}}_{\mathrm{cyl}}$ and $Q^{\mathrm{ideal}}_{\mathrm{MUT}} = Q^{\mathrm{ref}}_{\mathrm{cyl}}$ for the ideal operating conditions given in section 2.2. In general, Eqs. (7) and (8) incorporate the appropriate corrections to account for non-ideal effects. In the special case where flow conditions do not deviate substantially from ideal, the corrections for non-ideal effects are small relative to $\dot{m}^{\mathrm{ideal}}_{\mathrm{MUT}}$ and $Q^{\mathrm{ideal}}_{\mathrm{MUT}}$, and Eqs. (7) and (8) can be expressed as a product of near unity correction factors multiplied by the ideal flow.

3.1 Mass Flow and Volumetric Flow at the MUT near ideal conditions

When flow conditions are close to ideal, Eqs. (7) and (8) for mass flow and volumetric at the MUT simplify to

$$\tilde{\dot{m}}_{\mathrm{MUT}} = \left(\frac{\rho_{\mathrm{ref}} K^{\mathrm{ref}}_{\mathrm{V}} N_{\mathrm{e}}}{\Delta t}\right) R_1 R_2 R_3 R_4 R_5 S_1 S_2 S_3 S_4 S_5 S_6 \tag{9a}$$

and

$$\tilde{Q}_{\mathrm{MUT}} = \left[\frac{K^{\mathrm{ref}}_{\mathrm{V}} N_{\mathrm{e}}}{\Delta t}\right] R_1 R_2 R_3 S_1 S_2 S_3 S_4 S_5 S_6 G_1 G_2 \tag{9b}$$

where the near unity correction factors indicated by R_{i}'s, G_{i}'s, and S_{i}'s account for *reference condition corrections*, *gradient corrections*, and *storage corrections*, respectively. Expressions for these correction factors are given in Table 3 along with a description of their physical meaning. Equations (9a) and (9b) are derived by making the following modifications to Eqs. (7) and (8). First, the the swept volume ($\Delta V^{\mathrm{if}}_{\mathrm{cyl}}$) in Eqs. (7) and (8) is replaced by the product of $K^{\mathrm{ref}}_{\mathrm{V}}$ and N_{e} multiplied by the appropriate temperature correction factors specified in Eqs. (2), (3a), (3b), and (3c).[vi] Similar correction factors are used for the volume change in the connecting volume ($\Delta V^{\mathrm{if}}_{\mathrm{cv}}$).

[vi] For completeness elastic deformation of the cross sectional area attributed to forces induced by pressure stresses are included in Eqs (9a) and (9b).

The density expression in Eq. (4) is substituted for all of the density terms in Eqs. (7) and (8). The result of these substitutions for the volumetric flow, for example, is expressed as $Q_{\mathrm{MUT}} = Q_{\mathrm{MUT}}^{\mathrm{ideal}}\, y_{\mathrm{corr}}$ where $y_{\mathrm{corr}} = 1+\delta_{\mathrm{R}}+\delta_{\mathrm{G}}+\delta_{\mathrm{S}}$ is a first order Taylor series consisting of the deviation functions δ_{R}, δ_{G}, and δ_{S} that correct for non-idealities caused by reference condition effects, gradient effects, and storage effects. The deviation functions equal $\delta_{\mathrm{R,i}} = R_{\mathrm{i}} - 1$, $\delta_{\mathrm{G,j}} = G_{\mathrm{j}} - 1$, and $\delta_{\mathrm{S,k}} = S_{\mathrm{k}} - 1$ where R_{i}, G_{j}, and S_{k} are the correction factors in Table 3. For example, the first two reference condition deviation functions are $\delta_{R,1} = \alpha_{\mathrm{st}}\,(T_{\mathrm{en}} - T_{\mathrm{ref}})$ and $\delta_{R,2} = 2\,\alpha_{\mathrm{st}}\,(\hat{T}_{\mathrm{cyl}}^{\mathrm{i}} - T_{\mathrm{ref}})$. Provided that the deviation functions are small relative to unity ($\delta_{\mathrm{R,1}} << 1$, $\delta_{\mathrm{G,1}} << 1$, and $\delta_{\mathrm{S,1}} << 1$), higher order products of the deviations are negligible so that $y_{\mathrm{corr}} = (1+\delta_{\mathrm{R}})(1+\delta_{\mathrm{G}})(1+\delta_{\mathrm{S}})$ or $y_{\mathrm{corr}} = \prod R_{\mathrm{i}} G_{\mathrm{i}} S_{\mathrm{i}}$ is the product of the correction factors as indicated in Eqs. (9a) and (9b).

The R_{i}'s in Eqs. (9a) and (9b) correct the fluid density and the measured cylinder volume to the reference conditions. The G_{i}'s correct the flow when pressure and temperature gradients exist between the piston-cylinder assembly and the MUT. The S_{i}'s are *storage* corrections that account for a change in mass between the start and stop of the timing interval in the unswept region of the cylinder and in the connecting volume during a flow measurement.

For NIST operating conditions (which closely approximate ideal) many of the correction factors listed in Table 3 are essentially unity and have negligible impact on flow calculations. For clarity, we specify correction factors that can be neglected when using Eq. (9a) and (9b) in the remaining sections of the manuscript. Nevertheless, we have included these correction factors in Table 3 to provide guidance for field applications when operating conditions cannot be maintained as close to the ideal conditions. In this case, we point out that besides the list of correction factors in Table 3, one must also account for potential mechanical problems such as seal failure if a piston prover will be operated under extreme conditions.

Most of the correction factors in Table 3 require measurements of the average temperature and pressure at the start of the timed interval in both the cylinder and in the connecting volume (*e.g.*, $\hat{T}_{\mathrm{cyl}}^{\mathrm{i}}$, $\hat{T}_{\mathrm{cv}}^{\mathrm{i}}$, $\hat{P}_{\mathrm{cyl}}^{\mathrm{i}}$, and $\hat{P}_{\mathrm{cv}}^{\mathrm{i}}$). Since NIST data acquisition system is not currently equip to provide the time history of pressure and temperature measurements, time-averaged values are used (*i.e.*, $\tilde{T}_{\mathrm{cyl}}$, $\tilde{T}_{\mathrm{cv}}$, $\tilde{P}_{\mathrm{cyl}}$, and $\tilde{P}_{\mathrm{cv}}$) instead of the initial values. Insight to temperature and pressure stability is determined by monitoring the time-averaged temperatures and pressures throughout the entire calibration process. Typically, during a calibration the average temperatures and pressures remain nearly constant for repeated measurements at the same set point (*i.e.*, temperature stability less than 45 mK and pressure stability less than 0.1 %). The uncertainties introduced by these instabilities are incorporated in the uncertainty budget. A similar method is used to estimate the uncertainty attributed to storage effects (which are not corrected using the S_{i}'s in Table 3, but are included in the uncertainty budget). The most significant correction factor for storage effects is S_1 which contributes less than 0.01% to the uncertainty for a temperature change less than 100 mK. The uncertainty attributed to storage effects is calculated during a flowmeter calibration based on the measured temperature stability at the time of test.

Table 3. *Correction factors for mass flow in Eq. (9a) and volumetric flow in Eq. (9b).*

Region of Prover where Correction Applies	Correction Factors	Type of Correction	Description
Encoder	$R_1 = 1 + \alpha_{en}\left(T_{en} - T_{ref}\right)$	*Reference* Condition Correction	Axial change of encoder scale from the *reference* condition due to thermal expansion
Displaced Volume	$R_2 = 1 + 2\,\alpha_{st}\left(\hat{T}^{i}_{cyl} - T_{ref}\right)$	*Reference* Condition Correction	Radial change in the cylinder and shaft from *reference* condition due to thermal expansion
Displaced Volume	$R_3 = 1 + 2\,\varepsilon_{eff}\left(\hat{P}^{i}_{cyl} - P_{ref}\right)$	*Reference* Condition Correction	Radial change in cylinder and shaft from the *reference* condition due to internal fluid pressure[vii]
Displaced Volume	$R_4 = 1 - \beta\left(\hat{T}^{i}_{cyl} - T_{ref}\right)$	*Reference* Condition Correction	Change in the fluid density from the *reference* density (ρ_{ref}) due to thermal expansion
Displaced Volume	$R_5 = 1 + \kappa\left(\hat{P}^{i}_{cyl} - P_{ref}\right)$	*Reference* Condition Correction	Change in the fluid density from the *reference* density (ρ_{ref}) due to pressure change from P_{ref}
Displaced Volume/MUT	$G_1 = 1 - \beta\left(\hat{T}^{i}_{cyl} - \tilde{T}_{MUT}\right)$	Temperature *Gradient* Correction	Ratio density change between cylinder and MUT attributed to temperature difference between the cylinder and MUT
Displaced Volume/MUT	$G_2 = 1 + \kappa\left(\hat{P}^{i}_{cyl} - \tilde{P}_{MUT}\right)$	Pressure *Gradient* Correction	Ratio density change between cylinder and MUT attributed to pressure difference between the cylinder and MUT
Upswept Volume of Cylinder	$S_1 = 1 - \left(\frac{V^{f}_{cyl}}{N_e K^{ref}_{V}}\right)\beta\left(\hat{T}^{i}_{cyl} - \hat{T}^{f}_{cyl}\right)$	Mass *Storage*	Change in the fluid density in the unswept region of the cylinder due to a temperature change between the start and stop of a calibration
Upswept Volume of Cylinder	$S_2 = 1 + \left(\frac{V^{f}_{cyl}}{N_e K^{ref}_{V}}\right)\kappa\left(\hat{P}^{i}_{cyl} - \hat{P}^{f}_{cyl}\right)$	Mass *Storage*	Change in the fluid density in the unswept region of the cylinder due to a pressure change between the start and stop of a calibration
Upswept Volume of Cylinder	$S_3 = 1 + 2\left(\frac{V^{f}_{cyl}}{N_e K^{ref}_{V}}\right)\alpha_{st}\left(\hat{T}^{i}_{cyl} - \hat{T}^{f}_{cyl}\right)$	Mass *Storage*	Radial change in the unswept region of the cylinder and shaft diameters due to a temperature change between the start and stop of a calibration
Upswept Volume of Cylinder	$S_4 = 1 + 2\left(\frac{V^{f}_{cyl}}{N_e K^{ref}_{V}}\right)\varepsilon_{eff}\left(\hat{P}^{i}_{cyl} - \hat{P}^{f}_{cyl}\right)$	Mass *Storage*	Radial change in the unswept region of the cylinder and shaft diameters due to a pressure change between the start and stop of a calibration
Connecting Volume	$S_5 = 1 + \left(\frac{V^{ref}_{cv}}{N_e K^{ref}_{V}}\right)\left(3\alpha_{cv} - \beta\right)\left(\hat{T}^{i}_{cv} - \hat{T}^{f}_{cv}\right)$	Mass *Storage*	Change in the connecting volume and the density of fluid in this region due to a temperature change between the start and stop of a calibration[viii]
Connecting Volume	$S_6 = 1 + \left(\frac{V^{ref}_{cv}}{N_e K^{ref}_{V}}\right)\left(2\varepsilon_{cv} + \kappa\right)\left(\hat{P}^{i}_{cv} - \hat{P}^{f}_{cv}\right)$	Mass *Storage*	Mass storage in connecting volume attributed to pressure difference between start and stop of flow measurement

[vii] Note that ε_{eff} and ε_{cv} are parameters with units of inverse pressure to be determined using the appropriate pressure vessel equations in terms of the material modulus of elasticity, Poisson ratio, and cylinder or piping dimensions.

[viii] Note that α_{cv} is the linear coefficient of expansion for the connecting volume material.

4. Uncertainty Analysis

The method of propagation of uncertainty [8] as specified in the GUM [9] is used to determine the uncertainties of 1) the reference volumetric prover *K*-factor (K_V^{ref}) , 2) the volumetric flow at the MUT (Q_{MUT}), and 3) the mass flow at the MUT ($\dot{m}_{MUT}$). In all three cases the uncertainty sources are taken to be uncorrelated. The combined standard uncertainty (u_c) is determined by root-sum-squaring (RSS) the standard uncertainties (*i.e.*, 68 % confidence level or unity coverage factor, $k = 1$) multiplied by their sensitivity coefficients. The standard combined uncertainty is multiplied by a coverage factor of two ($k = 2$) to obtain the expanded uncertainty ($U = 2\,u_c$) at an approximate 95 % confidence level.

4.1 Determination of and Uncertainty of the Volumetric Prover K-factor (K_V^{ref})

The reference volumetric prover *K*-factor (K_V^{ref}) is determined using a water draw procedure at a reference temperature and pressure of $T_{ref} = 21$ ºC and $P_{ref} = 101.325$ kPa. After temperature equilibrium is established in the both the room and the fluid, the piston is slowly traversed through the cylinder and the displaced fluid is directed into a weigh tank instead of through the MUT. Thus, we determine K_V^{ref} using Eq. (9a) for mass flow with the exception that the total mass that would have passed through the MUT (*i.e.*, $\tilde{m}_{MUT}\,\Delta t$) is replaced by the buoyancy corrected and calibrated weigh scale readings. The resulting expression for K_V^{ref} is

$$K_V^{ref} = \frac{\left(M_T^f - M_T^i\right)\left(1-\rho_{air}/\rho_{ref}\right)^{-1}}{N_e \rho_{ref}\left(\prod_{n=1}^{5} R_n\right)\left(\prod_{n=1}^{6} S_n\right)}$$

or

$$K_V^{ref} = \frac{\left(M_T^f - M_T^i\right)\left(1-\rho_{air}/\rho_{ref}\right)^{-1}}{N_e \rho_{ref}\left[1-\beta(\hat{T}_{cyl}^i - T_{ref})\right]} \qquad (10)$$

where M_T^i is the tare weight of the empty collection vessel (after zeroing the scale), and M_T^f is the final scale reading after filling the collection vessel, and the quantity $\left(1-\rho_{air}/\rho_{ref}\right)^{-1}$ is the buoyancy correction. The air density (ρ_{air}) is calculated as a function of the pressure, temperature, and relative humidity in the room using the correlation developed by Jaeger and Davis. [10] During the measurement of K_V^{ref} the room temperature was controlled to within ± 2°C of T_{ref}, the fluid temperature was controlled to within ± 1°C of T_{ref}, and the fluid pressure was 101 kPa ± 1.5°kPa. For these conditions the only significant correction factor is $R_4 = 1-\beta(\hat{T}_{cyl}^i - T_{ref})$ as shown explicitly in Eq. (10). All of the other corrections for reference conditions and storage effects attribute less than 0.003 % to K_V^{ref} and are neglected.

The volumetric prover *K*-factor was measured on two occasions, first on April 2008, and a second time on Jan 2009. These measurements were done both with the piston moving to the left ($K_{V,left}^{ref}$) as well as with the piston stroking to the right ($K_{V,right}^{ref}$). On the first occasion the measurements of $K_{V,left}^{ref}$

and $K_{V,right}^{ref}$ were each repeated 20 times using Stoddard solvent as the working fluid. This data is denoted by the ×'s and +'s in Fig. 4. On the second occasion $K_{V,left}^{ref}$ was measured 5 times (×) while $K_{V,right}^{ref}$ was measured 8 times (+) using reverse osmosis water as the working fluid. The average of the twenty $K_{V,left}^{ref}$ and twenty $K_{V,right}^{ref}$ measurements made in Stoddard solvent are indicated in the figure by the solid line (—) and by the dotted line (····). Similarly, the averages of the five $K_{V,left}^{ref}$ and eight $K_{V,left}^{ref}$ measurements made in reverse osmosis water are indicated by the solid line (—) and dotted line (····) in the figure. The difference between the left and right average *K*-factor values in Stoddard solvent is 0.008 %, while the difference in reverse osmosis water is 0.002 %. Based on this good agreement we use the average volumetric *K*-factor, $K_V^{ref} = (K_{V,left}^{ref} + K_{V,left}^{ref})/2$ in all flow calculations, regardless if the piston is stroking left or right.

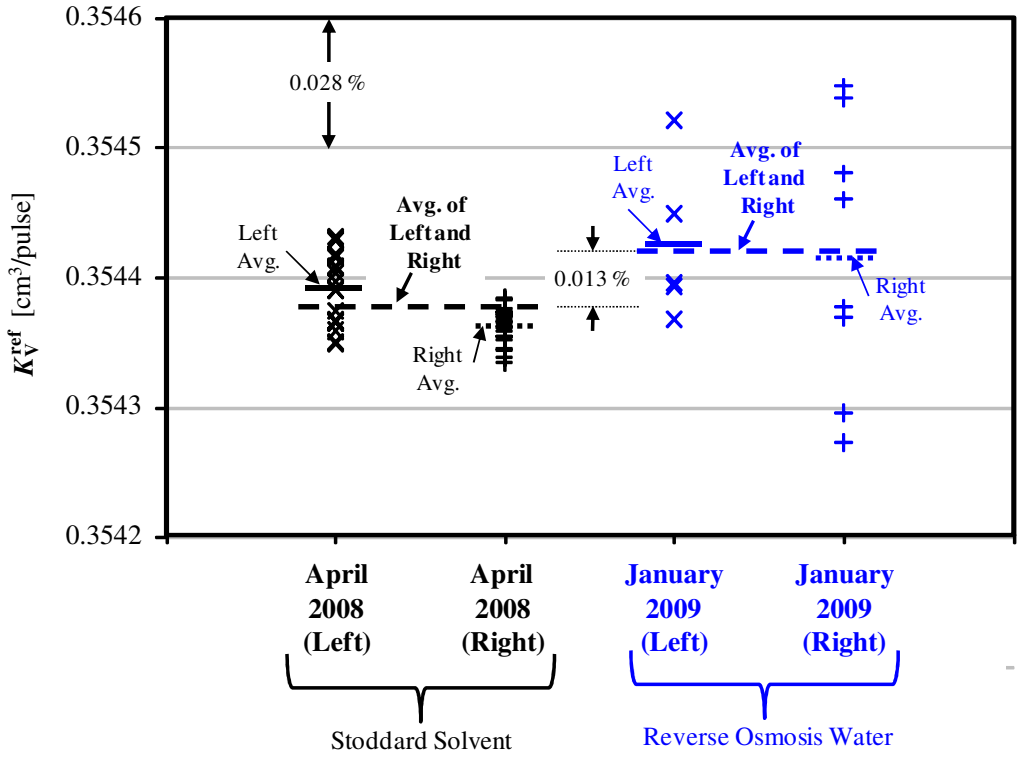

Figure 4. *Plot showing measurements of the volumetric prover K-factor done in April 2008 using Stoddard solvent and in January 2009 using reverse osmosis water.*

The dashed horizontal line (– – –) in Fig. 4 that connects the left and right *K*-factor measurements is the average K_V^{ref} for the April 2008 measurements in Stoddard solvent, and (– – –) is the average K_V^{ref} for the January 2009 measurements in reverse osmosis water. The difference between these two K_V^{ref} values is only 0.013 %, in spite of the January 2009 measurements being substantially noisier than those made in April 2008. We calculate the square of the combined standard uncertainty of the January 2009 *K*-factor measurements by

$$\left[\frac{u_c(K_V^{ref})}{K_V^{ref}}\right]^2 = \left[\frac{M_s^i}{K_V^{ref}}\frac{\partial K_V^{ref}}{\partial M_s^i}\right]^2\left[\frac{u(M_s^i)}{M_s^i}\right]^2 + \left[\frac{M_s^f}{K_V^{ref}}\frac{\partial K_V^{ref}}{\partial M_s^f}\right]^2\left[\frac{u(M_s^f)}{M_s^f}\right]^2 + \left[\frac{\beta}{K_V^{ref}}\frac{\partial K_V^{ref}}{\partial \beta}\right]^2$$
$$+\left[\frac{\rho_{ref}}{K_V^{ref}}\frac{\partial K_V^{ref}}{\partial \rho_{ref}}\right]^2\left[\frac{u(\rho_{ref})}{\rho_{ref}}\right]^2 + \left[\frac{\rho_{air}}{K_V^{ref}}\frac{\partial K_V^{ref}}{\partial \rho_{air}}\right]^2\left[\frac{u(\rho_{air})}{\rho_{air}}\right]^2 + \left[\frac{u(N_e)}{N_e}\right]^2 \qquad (11)$$
$$+\left[\frac{\hat{T}_{cyl}^i}{K_V^{ref}}\frac{\partial K_V^{ref}}{\partial \hat{T}_{cyl}^i}\right]^2\left[\frac{u(\hat{T}_{cyl}^i)}{\hat{T}_{cyl}^i}\right]^2 + \sigma_{left}^2 + \sigma_{right}^2 + \left|\frac{K_{V,left}^{ref} - K_{V,right}^{ref}}{K_{V,right}^{ref}\sqrt{3}}\right|^2$$

where σ_{left} and σ_{right} are the standard deviations of the repeated measurements for the piston stroking leftward and rightward. The last term is the percent difference between the piston stroking to the left versus to the right. The expanded uncertainty of the *K*-factor is $[U(K_V^{ref})/K_V^{ref}] = 0.073$ %. Table 4 itemizes the uncertainty of each component, specifying its overall percent contribution to the total uncertainty and the normalized sensitivity coefficients (*i.e.*, the derivative terms in Eq. 11).

Table 4. *Uncertainty budget for volumetric prover K-factor corresponding to Eq. (11) for January 2009 measurements using Reverse Osmosis Water.*

Vol. Prover *K*-factor	**Nom. Value**	**Rel. Unc. (k = 1)**	**Norm. Sen. Coeff.**	**Type A/B**	**Perc. Contrib.**	**Comments**
K_V^{ref} = 0.35442 [cm^3/pulse]	**[SI]**	**[%]**	**[ ]**	**[ ]**	**[%]**	
Initial Scale Mass, M_T^i [kg]	0	0.012	0.002	B	0	Control Charts of 60 kg scale
Final Scale Mass, M_T^f [kg]	13.8519	0.012	0.998	B	10.5	Control Charts of 60 kg scale
Water Density, ρ_{ref} [kg/m3]	997.855	0.0002	-1.002	B	0.0	Density of Reverse Osmosis Water[11]
Air Density, ρ_{air} [kg/m^3]	1.18	2	0.0015	B	0.7	Air Density [10] and measured T, P, and RH
Encoder Pulse, N_e [pulse]	39170	0	-1	B	0.0	Integer number of pulses (assumes no pulses missed)
Thermal Expan. Coeff. for Water at 21 ℃; β [1/°C]	0.00022	10	0.0001	B	0.0	Variation with Temp. betwn 19 ℃ to 23 ℃ (rect. dist assumed)
Initial Fluid Temp., T_{cyl}^i [°C]	21.63	0.02	0.06	B	0.1	Cal. Records and spatial non-uniformity of 6 thermistors
Repeat. Meas. of $K_{V,left}^{ref}$ [cm^3/pulse]	N/A	0.017	1	A	22.6	Std. dev. of 5 meas.
Repeat. Meas. of $K_{V,right}^{ref}$ [cm^3/pulse]	N/A	0.03	1	A	66.0	Std. dev. of 8 meas.
Diff. betwn. $K_{V,left}^{ref}$ and $K_{V,right}^{ref}$	N/A	0.001	1	B	0.1	Rect. Dist. Assumed
Combined Std. Unc. (k = 1) =	**0.0365 %**				**100**	**68 % confidence interval**
Expanded Unc. (k = 2) =	**0.073 %**				**100**	**95 % confidence interval**

4.2 Uncertainty of the Volumetric and Mass Flow at the MUT

The volumetric flow at the MUT is determined using Eq. (9b). The square of the combined standard uncertainty of the volumetric flow at the MUT is calculated by

$$\begin{aligned}\left[\frac{u_c\left(\tilde{Q}_{\mathrm{MUT}}\right)}{\tilde{Q}_{\mathrm{MUT}}}\right]^2 = &\left[\frac{u\left(K_{\mathrm{V}}^{\mathrm{ref}}\right)}{K_{\mathrm{V}}^{\mathrm{ref}}}\right]^2 + \left[\frac{u(N_{\mathrm{e}})}{N_{\mathrm{e}}}\right]^2 + \left[\frac{u(\Delta t)}{\Delta t}\right]^2 + \left(\frac{\tilde{T}_{\mathrm{MUT}}}{\tilde{Q}_{\mathrm{MUT}}}\frac{\partial \tilde{Q}_{\mathrm{MUT}}}{\partial \tilde{T}_{\mathrm{MUT}}}\right)^2\left[\frac{u\left(\tilde{T}_{\mathrm{MUT}}\right)}{\tilde{T}_{\mathrm{MUT}}}\right]^2 \\ &+ \left(\frac{T_{\mathrm{en}}}{\tilde{Q}_{\mathrm{MUT}}}\frac{\partial \tilde{Q}_{\mathrm{MUT}}}{\partial T_{\mathrm{en}}}\right)^2\left[\frac{u(T_{\mathrm{en}})}{T_{\mathrm{en}}}\right]^2 + \left(\frac{\hat{T}_{\mathrm{cyl}}^{\mathrm{i}}}{\tilde{Q}_{\mathrm{MUT}}}\frac{\partial \tilde{Q}_{\mathrm{MUT}}}{\partial \hat{T}_{\mathrm{cyl}}^{\mathrm{i}}}\right)^2\left[\frac{u\left(\hat{T}_{\mathrm{cyl}}^{\mathrm{i}}\right)}{\hat{T}_{\mathrm{cyl}}^{\mathrm{i}}}\right]^2 \\ &+ \left(\frac{\hat{P}_{\mathrm{cyl}}^{\mathrm{i}}}{\tilde{Q}_{\mathrm{MUT}}}\frac{\partial \tilde{Q}_{\mathrm{MUT}}}{\partial \hat{P}_{\mathrm{cyl}}^{\mathrm{i}}}\right)^2\left[\frac{u\left(\hat{P}_{\mathrm{cyl}}^{\mathrm{i}}\right)}{\hat{P}_{\mathrm{cyl}}^{\mathrm{i}}}\right]^2 + \left(\frac{\tilde{P}_{\mathrm{MUT}}}{\tilde{Q}_{\mathrm{MUT}}}\frac{\partial \tilde{Q}_{\mathrm{MUT}}}{\partial \tilde{P}_{\mathrm{MUT}}}\right)^2\left[\frac{u\left(\tilde{P}_{\mathrm{MUT}}\right)}{\tilde{P}_{\mathrm{MUT}}}\right]^2 \\ &+ \left(\frac{\beta}{\tilde{Q}_{\mathrm{MUT}}}\frac{\partial \tilde{Q}_{\mathrm{MUT}}}{\partial \beta}\right)^2\left[\frac{u(\beta)}{\beta}\right]^2 + \left(\frac{\alpha_{\mathrm{en}}}{\tilde{Q}_{\mathrm{MUT}}}\frac{\partial \tilde{Q}_{\mathrm{MUT}}}{\partial \alpha_{\mathrm{en}}}\right)^2\left[\frac{u(\alpha_{\mathrm{en}})}{\alpha_{\mathrm{en}}}\right]^2 \\ &+ \left(\frac{\alpha_{\mathrm{st}}}{\tilde{Q}_{\mathrm{MUT}}}\frac{\partial \tilde{Q}_{\mathrm{MUT}}}{\partial \alpha_{\mathrm{st}}}\right)^2\left[\frac{u(\alpha_{\mathrm{st}})}{\alpha_{\mathrm{st}}}\right]^2 + \left(\frac{\kappa}{\tilde{Q}_{\mathrm{MUT}}}\frac{\partial \tilde{Q}_{\mathrm{MUT}}}{\partial \kappa}\right)^2\left[\frac{u(\kappa)}{\kappa}\right]^2 .\end{aligned} \tag{12}$$

Table 5 itemizes each component of uncertainty. The expanded uncertainty in volumetric flow at the MUT is $[U(Q_{\mathrm{MUT}})/Q_{\mathrm{MUT}}] = 0.074$ %. The uncertainty is valid over the entire flow range from 1.1 lmp to 151 lpm. As expected the majority of the uncertainty is attributed to the measurement of the reference volumetric prover *K*-factor. The uncertainty in mass flow at the MUT is determined in an analogous fashion. In this case the measurement of the Stoddard solvent density slightly increases the mass flow uncertainty above the volumetric flow uncertainty. The total uncertainty of determining the Stoddard solvent density (including contributions from the reference corrections R_4 and R_5 in Table 3, but omitting G_1 and G_2) is 0.016 % ($k = 1$) so that the expanded mass flow uncertainty at the MUT is $[U(\dot{m}_{\mathrm{MUT}})/\dot{m}_{\mathrm{MUT}}] = 0.08$ % ($k = 2$).

Table 5. *Uncertainty budget for volumetric flow at MUT corresponding to Eq. (12)*

Vol. Flow; Q_{MUT} [lpm]	**Nom. Value**	**Rel. Unc. (k=1)**	**Norm. Sen. Coeff.**	**Type A/B**	**Perc. Contrib.**	**Comments**
Q_{MUT} = 113.56 lpm	[SI]	[%]	[ ]	[ ]	[%]	
Volumetric Prover K-factor, K_V^{ref}, [cm^3/pulse]	0.35442	0.036	1	B	96.8	see Table 4
Duration of Piston Stroke; Δt [s]	6.1	0.002	-1	B	0.3	Control Charts for Freq. Calib.
Encoder Pules; N_e [pulse]	32410	0.0	1	B	0.0	Integer number of pulses (assumes no pulses missed)
Temp. Encoder; T_{en} [°C]	23	0.02	0.0002	B	0.0	Env. Sensor Calib. Records
Initial Fluid Temp., T_{cyl}^{i} [°C]	22	0.02	0.02	B	0.0	Temp. Cal. Records and spatial non-uniformity of 6 thermistors
Temp. at the MUT; T_{MUT} [°C]	21.75	0.017	-0.02	B	0.0	Temp. Cal. Records and spatial non-uniformity of 6 thermistors
Pres. at the MUT; P_{MUT} [kPa]	240	0.2	0.0002	B	0.0	Pres. Calib. Records
Pres. at the cylinder; P_{cyl}^{i} [kPa]	250	25	0.0002	B	2.5	Estimate of worst case pres. drop; (rect. dist. assumed)
Linear Thermal Expan. Coeff. of Stainless Steel; α_{st} [1/°C]	1.7E-05	5	3E-05	B	0.0	see Reference [4, 5]
Isothermal Comp. Factor for Stoddard solvent at ; κ [1/kPa]	9.3E-07	7	0.0002	B	0.0	See Reference [7]
Thermal Expan. Coeff. of Stoddard Solvent, β [1/°C]	0.00097	10	0.0002	B	0.4	Fit residuals from the measured density using a vibrating tube densimeter
Linear Thermal Expan. Coeff. of Encoder; α_{en} [1/°C]	0.000008	5	1.6E-05	B	0.0	see Reference [5]
Combined Std. Unc. (k = 1) =	**0.037 %**			**100**		**68 % confidence interval**
Expanded Unc. (k = 2) =	**0.074 %**			**100**		**95 % confidence interval**

5. Comparison of Calibration data between the 20 L HLFS and other NIST flow standards

5.1 Calibration Procedure

To begin a calibration the MUT is installed in the test section, and the calibration fluid is pressurized to the desired level. Next, an air bleed is performed to remove any air that entered the system during installation of the MUT. After the fluid and room temperatures are brought to equilibrium at T_{ref}, a custom software package is used to control the calibration process. Typical calibrations measure the flow at six set points (*i.e.*, 5 %, 15 %, 30 %, 50 %, 70 %, and 100 % of the full scale flow). Each of the six flows is measured on two occasions with 5 repeats on each occasion. The final calibration result for each set point is the average of at least 10 measurements. The standard deviation of the 10 measurements is taken to be the reproducibility.

For turbine meters the calibration data is plotted in the dimensionless units of Roshko and Strouhal numbers where the Rosko number is defined as

$$Ro = \frac{\mathcal{D}^2 f}{\nu}. \tag{13}$$

Here, f is the blade frequency, $\mathcal{D} = \mathcal{D}_{\text{ref}}[1+\alpha_{\text{MUT}}(\tilde{T}_{\text{MUT}} - T_{\text{ref}})]$ is the temperature corrected diameter of the MUT, and $\nu = \nu_{\text{ref}}[1+a_1(\tilde{T}_{\text{MUT}} - T_{\text{ref}})]$ is a curve fit of the fluid kinematic viscosity determined experimentally using a capillary viscometer. The Strouhal number is defined by

$$St = \frac{\pi \mathcal{D}^3 f}{4Q_{\text{MUT}}} \tag{14}$$

where $\tilde{Q}_{\text{MUT}}$ is determined by Eq. (9b).

5.2 Internal Comparison Results with other NIST flow standards

The 20 L HLFS uncertainty calculations were verified by comparison to the other three liquid hydrocarbon standards in Table 1 using Stoddard solvent as the working fluid. In addition the 20 L HLFS was compared to the water flow facility. The same dual rotor turbine meter was used as the transfer standard for all of the comparisons. The flow comparisons spanned a flow range from 3.8 lpm to 38 lpm. The comparison results are plotted in Figure 5 where the symbols in the legend indicate the measured data. The solid line (——) is a curve fit of 13 different calibrations done in Stoddard solvent over a six month period using the 20 L HLFS. The two dashed lines (– – –) are the 95 % confidence interval of the curve fit. The results show all five of NIST's primary flow standards agreed within their uncertainties. In addition, the repeated calibrations of the turbine meter over a 6 month period demonstrate the stability of the 20 L HLFS.

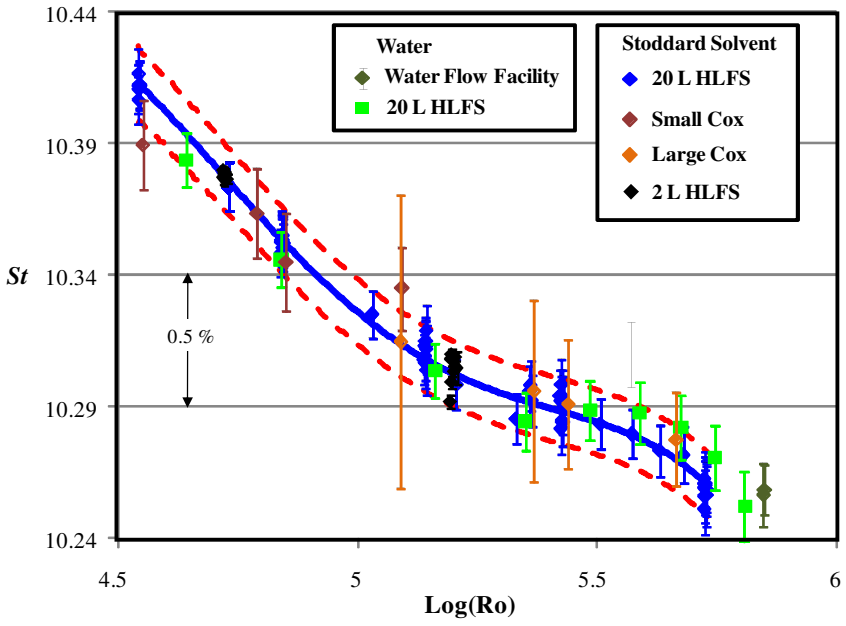

Figure 5. *Comparison results between five NIST liquid flow standards including the four hydrocarbon flow standards in Table 1 and NIST's water flow standard.*

6. Summary and Conclusions

This manuscript documents the performance and uncertainty of NIST 20 L HLFS. This primary standard is used to provide flow traceability to NIST customers for hydrocarbon liquid flows. Based on the uncertainty analysis herein the volumetric flow uncertainty is 0.074 % ($k = 2$) and the mass flow uncertainty is 0.08 % ($k = 2$). The comparison of the 20 L HLFS with 3 other hydrocarbon liquid flow standards and a water flow standard are consistent with the above uncertainty analysis. In addition, the comparison shows that all of the standards are in agreement within their stated uncertainties. Finally, the manuscript introduced a set of correction factors that can be used to estimate uncertainties of other liquid piston prover flow standards.

Acknowledgements
The technical contributions from Sherry Sheckels and John D. Wright are gratefully acknowledged. Special acknowledgement is given to Iosif Shinder for calibrating the turbine meter transfer standard against the NIST water flow standards.

REFERENCES

[1] Yeh T. T., Aguilera, J., and Wright, J. D., *Hydrocarbon Liquid Calibration Service*, NIST Special Publication 250-1039, 2009.

[2] Yeh T. T., Aguilera, J., and Espina, P. I., Mattingly, G. E., Briggs, N. R., *An Uncertainty Analysis of A NIST Hydrocarbon Liquid Flow Calibration Facility*, Proceedings of Heat Transfer/Fluids Engineering Summer Conference, Charlotte, North Carolina, July 11-15, 2004.

[3] Shinder, I. I., and Moldover, M. R., *Dynamic Gravitational Standard for Liquid Flow: Model and Measurements*, 7th International Symposium on Fluid Flow Measurement, Anchorage, AK , August 12-14, 2009.

[4] Lide, D. R., *CRC Handbook of Chemistry and Physics 73rd Ed.*, CRC Press, Inc., Boca Raton, FL. 1992

[5] Benson, W., Harris, J. W., Stocker, H., Lutz, H., *Handbook of Physics*, Springer, New York, NY, 2006.

[6] Mattingly, G. E., *The Characterization of a Piston Displacement-Type Flowmeter Calibration Facility and the Calibration and Use of Pulsed Output Type Flowmeters*, Journal of Research of the National Institute of Standards and Technology, Vol. 97, No. 5, Pg. 509, September-October 1992.

[7] API, *Manual of Petroleum Measurement Standards*, Chapter 4.3: Proving Systems - Small Volume Provers", 1st ed. (American Petroleum Institute, Washington, D.C., 1993).

[8] Coleman, H. W., and Steele, W. G., *Experimentation and Uncertainty Analysis for Engineers*, John Wiley and Sons, Inc., New York, NY, 1989.

[9] Taylor, B. N. and Kuyatt C. E., *Guidelines for the Evaluating and Expressing the Uncertainty of NIST Measurement Results*, NIST TN-1297, MD,1994.Pressure vessel equation.

[10] Jaeger K. B., Davis R. S., *A Primer for Mass Metrology*, NBS (U.S.), Spec. Publ. 700-1, Industrial Measurement Series, 79 p. 5, 1984.

[11] Patterson, J. B. and Morris, E. C.*, Measurement of absolute water density, 1°C to 40°C*, Metrologia, 31, 277, 1994.